Journal of Applied Physics ARTICLE scitation.org/journal/jap

Impact of visible light and humidity on the stability of high-power light emitting diode packaging material

Cite as: J. Appl. Phys. **130**, 083101 (2021); doi: 10.1063/5.0059515
Submitted: 9 June 2021 · Accepted: 6 August 2021 ·
Published Online: 24 August 2021

Abdul Shabir[1,2] and Cher Ming Tan[1,2,3,4,a)]

AFFILIATIONS

[1]Centre for Reliability Science and Technology, Chang Gung University, Wenhua 1st Road, Guishan Dist., Taoyuan City 33302, Taiwan
[2]Department of Electronics Engineering, Chang Gung University, Wenhua 1st Rd., Guishan Dist., Taoyuan City 33302, Taiwan
[3]Department of Urology, Chang Gung Memorial Hospital, Guishan, Taoyuan 333, Taiwan
[4]Centre for Reliability Engineering, Ming Chi University of Technology, 84 Gungjuan Rd., Tishan Dist., New Taipei City 24301, Taiwan

[a)]**Author to whom correspondence should be addressed:** cmtan@cgu.edu.tw

ABSTRACT

There are many advantages of LEDs in energy and environmental conservation, but their short life in many outdoor applications prompt a necessity to have a detailed understanding of their degradations to prolong their lifetime, which can also conserve LED material and even expand their applications. Using *ab initio* density functional theory formulation, we identify the detail paths of the LED degradation in outdoor applications. We discovered that the main stressors are humidity and the light that is emitted from the LED chip itself. This is rather ironical. A mathematical model is developed based on the *ab initio* study, and excellent experimental agreements are found. With this model, we can predict the situations where no and slow degradations can be achieved, and these are verified experimentally here. We can also predict quantitatively the time to a specific degradation severity. Quality index of the housing material for LEDs can also be determined.

I. INTRODUCTION

High-power light emitting diodes (LEDs) are increasingly important light sources due to their high efficacy in the conversion of electrical power to light energy, and this is a key step in energy conservation for the globe. In 2017, when the use of LED lighting was 26% worldwide, energy savings of 1.1 quadrillion Btu in the U.S. leading to cost savings equivalent to 12 billion USD was reported by an office of the U.S. Department of Energy.[1,2] They are also mechanically robust and do not emit UV and, therefore, are used commonly for various outdoor applications. However, rapid LED degradations are commonly observed in outdoor applications that render their short lifetimes,[3–5] where their reduced light output and color changes could lead to potential traffic accidents, safety of pedestrians, and commercial lawsuits such as the recently case in Detroit, USA.[6]

With the advantages of LEDs in energy and environmental conservation, a detailed understanding of their degradations in outdoor applications will be beneficial to prolong their lifetime so that LED material conversation can also be possible with even wider applications. It is with this motivation that this work is produced.

All high-power white LEDs contain semiconductor multiple quantum well structures that emit either blue or UV light.[7–10] We focus on the blue LEDs in this study. A phosphor layer is placed on top of the semiconductor chip to down-convert the blue light into yellow light, or quantum dot layers are also used to down-convert the blue light to green and red light,[11–18] and white light then results from the mix of these wavelengths of light. These materials are placed in a housing make of silicone, and the entire structure is encapsulated using a different type of silicone for their protection against external environments; they also act as lens for the emitted lights. Silicone is used here owing to its properties including thermal and chemical stability, thermal insulation, hydrophobicity, low surface tension, and low flammability.[19] These properties are attributed by the strong inorganic silicon–oxygen backbone of the silicone polymers.[20] Most of the silicone polymers are based on polydimethylsiloxane (PDMS) and its co-polymers.

Although PDMS polymers are stable, extreme environments can cause its deterioration affecting its usefulness. A study by Lewis reported that water reacts slowly with PDMS at 150 °C without a catalyst,[21] and equilibrium was reached after 3 months, with the activation energy (E_a) for hydrolysis of the Si–O bond found to be 96.23 kJ mol^{-1}. A recent study on the deterioration of PDMS in LED housing found that the degradation mechanisms follow a path of hydrolysis, condensation, thermal oxidation, and thermal aging when it was exposed to 85 °C temperature in the presence of moisture and with LEDs turned on.[22] The hydrolysis and condensation reactions in PDMS led to its discoloration, and thermal oxidation and thermal aging led to the formation of cracks on the PDMS material. Such degradation process leads to significant decrease in the luminous flux of LEDs, which in turn degrades the performance of LEDs.[22] On the other hand, under the same environmental condition, but with LEDs turned off, no deterioration of silicone was observed.[23] Therefore, it clearly reveals that visible light has a significant impact on the degradation of silicone. Experiments have also shown that no such degradation occurs when the LEDs are powered on in a low humid environment.[24] Therefore, the PDMS degradation under outdoor environments can be traced to the presence of humidity and light and their impacts are to be explored quantitatively.

As material degradation is governed by thermodynamics and kinetics, first-principles density functional theory (DFT) is used for such exploration. DFT is a reliable method for predicting intermediate groups, transition states (TSs), and atomic structures in a chemical reaction.[25–28] VASP (Vienna *ab initio* simulation package) is used in this work.

II. SIMULATION RESULTS AND IMPLICATIONS

The course of hydrolysis of PDMS is shown in Fig. 1(a). The first intermediate stage B [Fig. 1(a)] corresponds to a ΔG of 22.6 kJ mol^{-1}. This energy change is believed to be the sum of the dissociation energy of an H_2O molecule present within the PDMS polymer and the energy required for the cleavage of the Si–O–Si bond from the PDMS polymer. The dissociation energy (D_e) of H_2O predicted theoretically while accounting for the zero-point vibrational energy (ZPVE) was 13.8 kJ mol^{-1} with an estimate error of ±0.4 kJ mol^{-1} by MP2 CCSD and CCSD(T) calculations,[33] and the energy for the cleavage of the Si–O–Si bond with an H_2O molecule as calculated by DFT methods was 12.2 kJ mol^{-1} as mentioned elsewhere.[34] In fact, the cleavage of the Si–O–Si bond occurs mainly in two ways: a homolytic cleavage and water assisted cleavage.[20] The energy for cleavage of the Si–O–Si bond varies in a wide range from 12.2 to 161.9 kJ mol^{-1} depending on the associated functional groups with the Si–O–Si backbone.[34–40]

According to the transition state theory (TST), an intermediate corresponding to a high ΔG and in highly unstable equilibrium can be identified as a transition state (TS) for a particular reaction.[41] Theoretical calculation of hydrolysis of dimethylsilane-diol in literature studies found that the TS of hydrolysis reaction has a pentavalent co-ordination of the silicon atoms,[42] and this is depicted only in the stage showed as (C) in Fig. 1(a) of the reaction in our simulation result with ΔG of the transition state (TS) calculated to be 123.2 kJ mol^{-1}. The conversion of π to π* orbitals in a silicon atom as well as an oxygen atom of the terminal siloxane group is found to take place in this step. This conversion from bonding to anti-bonding

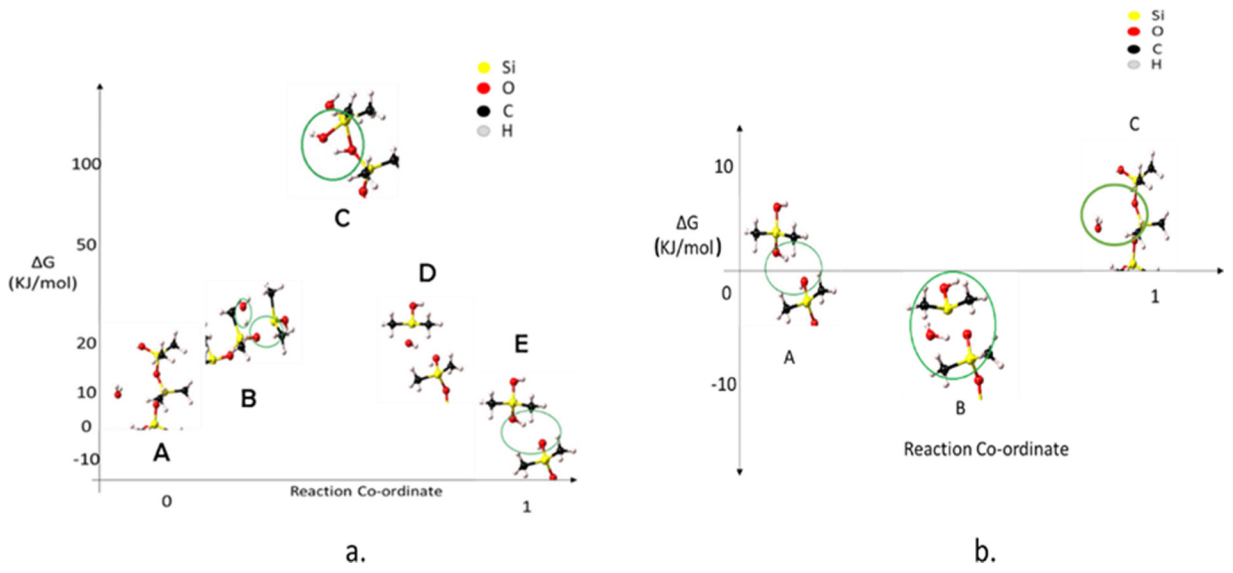

FIG. 1. (a) The minimum energy path (MEP) and related intermediates of the hydrolysis reaction traced from transition state search computation based on DFT. The *y* axis is the change in Gibb's free energy and the *x* axis represents the reaction coordinates. The initial step of the reaction (A) is set at 0.0 kJ mol^{-1}, and thus the energy barriers at each stage of the reaction can be considered Gibb's free energy change (ΔG) for the stage. (b) The minimum energy path of condensation reaction traced from transition state search computation based on DFT. *x* and *y* axes are the same as (a).

orbitals in a silicon atom led to its pentavalent co-ordination state and a trivalent co-ordination state on the bonded oxygen atom as reported elsewhere.[42,43] The terminal silicon atom forms an extra bond with a hydroxyl group and the trivalent co-ordination state of oxygen occurs with the formation of an extra H-bonding along with its two Si bonds. The ΔG of 123.2 kJ mol^{-1} associated with the TS represents the activation energy of the hydrolysis.[42]

De-polymerization of the transition state intermediate takes place where a ΔG of 20.4 kJ mol^{-1} is calculated for the intermediate (D) in Fig. 1(a). This calculated energy (ΔG) is significantly lower than its preceding steps indicating that the intermediate observed is comparatively more stable than its previous intermediates. De-polymerization leads to two Si–O cleavages in the TS molecular intermediate. The molecular structure in this stage is also similar to the structure (B) in Fig. 1(a) with a rearrangement of the H and OH ions after Si–O–Si bond cleavage takes place. To neutralize the ionic state, the H-ion near the Si bonded O-ion will reposition itself and lead to an O–H bond formation. The complex formed was decamethyl-1,9-pentasiloxanediol, which is the final structure (E) after hydrolysis. The unstable Si atom in the siloxanol monomer is also stabilized by the formation of the fourth bond between the Si atom and hydroxyl group. The new compound obtained is identified as monomeric silanediol. This stage of reaction was found to be highly spontaneous as compared to the ormer stages of the reaction as the calculated ΔG for this reaction step is −7.5 kJ mol^{-1}. Similar transformation was also observed in the proton-NMR studies of the hydrolysis of oligodimethylsiloxane-a,ω-diols, which indicated that the chemical equilibrium shifts toward the monomer-diol as mentioned elsewhere.[44]

From Gibb's free energy point of view, the product after hydrolysis reaches a comparative equilibrium stage, but it does not attain stable equilibrium as $\Delta G \neq 0$.[45] This implies that the silanediol monomer and siloxane oligomer would undergo further changes for a possible chemically stable equilibrium state. Varaprath *et al.*[46] reported that silanol monomers or oligomers readily undergo condensation or dimerization to form polymeric siloxanes. Mono-hydroxyl silicon species undergo dimerization, and di-hydroxyl silicones will form linear and cyclic polymers while three or more hydroxyl functions would yield three-dimensional network polymers or resins. It was also reported that condensation of siloxanes is rapid in the presence of acidic or basic catalysts.[46] Using the end product of hydrolysis as the initial structure for the condensation reaction of PDMS, the minimum energy path (MEP) can be obtained using DFT study, and it is shown in Fig. 1(b).

The calculated ΔG of the transition state (TS) (B) in Fig. 1(b) is found to be −6.9 kJ mol^{-1}, which indicates that silanols can spontaneously undergo condensation reaction.[46] The silanols from the first stage of the reaction undergoes rearrangement by dissociating an H-ion and hydroxyl group from both the structures in TS. These dissociated ions recombine to form a water molecule while leaving the Si atoms in both structures in a trivalent co-ordination state, which makes them ionic.

Upon calculation of enthalpy of formation (ΔH_f) of the chemical intermediates both before and after hydrolysis, it was found that 459.85–459.7 kJ mol^{-1} of energy is absorbed during the transformation when the hydrolysis takes place at temperatures between 298 and 458 K. The temperature limit chosen for the calculation here is in accordance with the experiments to be performed as described in Sec. II and Table I in the Appendix. This amount of energy absorbed indicates that hydrolysis is an endothermic process, which is in agreement with the thermogravimetry/differential thermal analysis (TG/DTA) analysis as mentioned elsewhere.[47] On the other hand, the analysis of ΔH for the condensation reaction found that energy release varying between 459.7 and 544.9 kJ mol^{-1}. The release of energy on condensation implies an exothermic process, which increases the cross-link density of PDMS.

In general, negative activation energy is not observed for any elementary reaction as it is not in accordance with the Arrhenius reaction. However, in the case of a reaction which is composed of several steps, there is a possibility of negative activation energy.[48,49] In these cases, there is a rapid pre-equilibrium step, which is exothermic in nature, and the condensation reaction investigated here fits into such category.

Our investigation provides important detail insights into the mechanisms of hydrolysis and condensation. To initiate the hydrolysis reaction experimentally, external energy will be required as its activation energy is 123.24 kJ mol^{-1}. Owing to the negative activation energy of the condensation reaction, once the hydrolysis reaction occurs, condensation will follow spontaneously. Also, hydrolysis is an endothermic reaction, whereas condensation reaction is an exothermic reaction, which is in agreement as found experimentally.[22] Therefore, when hydrolysis and condensation occur gradually on a PDMS surface, the energy released by condensation would further be absorbed by the nearby un-hydrolyzed PDMS surfaces to initiate hydrolysis in the presence of moisture. As more energy is provided by the condensation reaction, the externally supplied energy will trigger more hydrolysis, making the hydrolysis proceed even faster as there is an increasing excess energy to trigger the hydrolysis reaction, and the rate of hydrolysis and condensation will increase with time. The higher the externally supplied energy, the faster will be the reaction rates increase with time. Furthermore, the energy required to initiate hydrolysis is 22 kJ mol^{-1} as found in our calculations [Fig. 1(a)]. The maximum energy supplied by temperature at 85°C is only 5.71 kJ mol^{-1}, which is not sufficient to initiate hydrolysis reaction. This explains that temperature and humidity without any light do not cause the hydrolysis of silicone to occur as observed experimentally.[23]

To derive a quantitative model based on the above understanding, let us denote V_d as the discolored volume due to hydrolysis and condensation. It is to be noted that before the silicone discolored, very little light will be absorbed by the silicone as this is the very reason for having the material as LED packaging. As more light is absorbed by the discolored volume, more externally supplied energy will become available for hydrolysis and the discolored volume will grow over time.

From the above understanding of the degradation physics of PDMS, there are three energy sources that can contribute to the increase in V_d, namely, the LED temperature, the blue and yellow light wavelength (our later experimental samples are the LEDs with yellow phosphor), and the heat released from the condensation reaction. The detailed derivation is shown in the Appendix. The

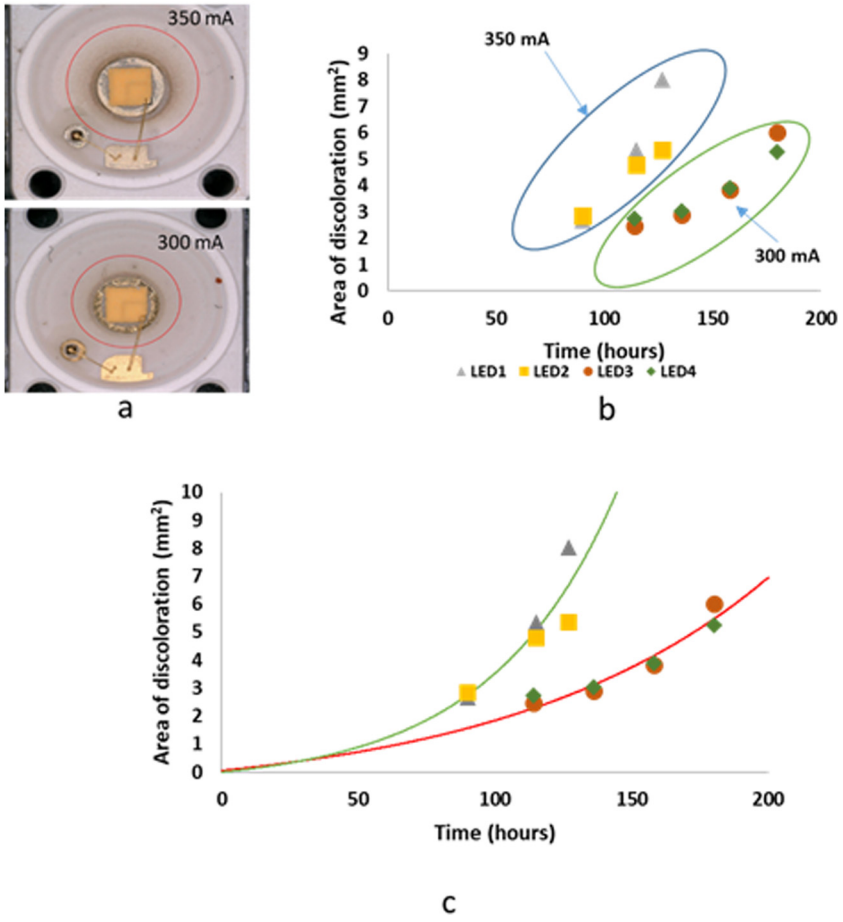

FIG. 2. (a) Radius of discoloration at different drive currents (indicated on the Keyence VHX5000 microscope at 50× magnification). (b) Trends of areas of discoloration of PDMS at different input currents. (c) Model fitting (solid line) with experimental data for the case of 350 and 300 mA drive currents.

quantitative model of the growth of the discolored area with time in the presence of temperature, humidity, and light is given as

$$A_d(t) = A_0 + A_2 e^{A_1 t}, \tag{1}$$

where $A_1 = \frac{\sum_{i=1}^{2} \beta_i P_i}{\alpha}$.

P_1 represents the power density of the blue light and P_2 represents the power density of the yellow light. The corresponding β represents the absorption coefficient of the different light by the discolored region, respectively, which we assumed to be constant in this work. As the discolored region is dark brown in color, we can consider all the blue light is absorbed, i.e., $\beta_1 = 1$. $\alpha = \left(k_1 E_a - \frac{k_B T}{V} - \alpha_{cond}\beta_3\right)\delta$; δ is the effective penetration depth of the lights. The meaning of other parameters can be found in the Appendix. At a given ambient temperature, α is approximately a constant. A_2 is related to the quality of the silicone. Specifically, if the silicone has lager pore size or trapped particles that can absorb light, the value of A_2 will be larger. $A_0 = -A_2$.

III. VERIFICATION OF QUANTITATIVE MODEL

Significant discoloration of the PDMS is observed for the two set of LEDs as shown in Fig. 2(a). Our experiments found that LEDs stressed at 350 mA have the radius of discoloration ≈1600 μm in 127 h, whereas the radius is ≈1389 μm for the LEDs stressed at 300 mA after 180 h. This agrees with our model that the rate of discoloration is higher for higher light intensity, which is a function of the current supplied to the LEDs. The time variation of the areas of discoloration of the PDMS is shown in Fig. 2(b). The stop time for the 350 and 300 mA conditions are 127 and 180 h, respectively. The corresponding lumen output for both the cases is around 10%, which is well below the reliability test standards of LM-70. From our model, it is clear that if hydrolysis and condensation can be prevented or delayed during the early usage time of the LED, the lifetime of the LEDs can be extended.

Figures 2(c) and 2(d) show excellent fitting of our quantitative model in Eq. (1) with experimental data. The parameters of our models for the two cases are shown in Table II in the Appendix.

The Eyring and Polanyi model[50] shown in Eq. (2) is used for the estimation of activation energy from experimental data,

$$r = \frac{\tau K_B T}{h} e^{\frac{-\Delta G}{RT}}. \tag{2}$$

Here, r is the rate of reaction, τ is the transmission coefficient,

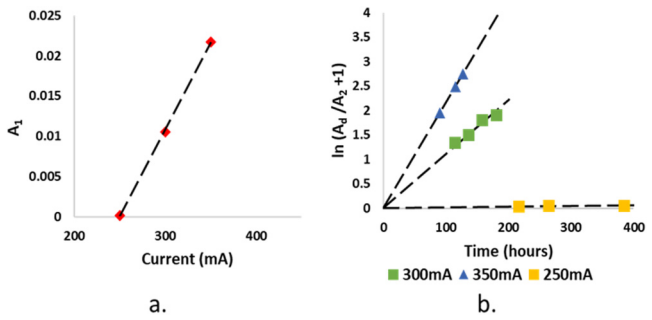

FIG. 3. (a) Values of A_1 in the quantitative model for different LED drive currents. The drive current is directly proportional to the light intensity of the LED as can be seen in Figs. 6 and 8 in the Appendix. One can see a perfect linear fit of the data as expected from the model developed in this work. (b) Plot of $\ln\left(\frac{A_d}{A_2}+1\right)$ vs time for different LED drive currents. A perfect linear fit is observed as expected from the model developed. Values of A_1 and A_2 are obtained by fitting the experimental data of A_d with Eq. (1).

which is often taken as unity implying all reactants are converted into products after the transition state, K_B is Boltzmann's constant, h is Planck's constant, and ΔG is the free energy of activation. T is the total LED temperature.

Experimentally, the rate of reaction (r) can be computed as a rate of silicone discoloration due to hydrolysis and condensation reactions. However, as the condensation reaction occurs very fast as shown in our DFT calculation, the apparent activation energy should likely resemble that of the hydrolysis reaction. Rewriting Eq. (2) as $\Delta G_{expt} = -RT\ \ln(rh/tKT)$ and substituting the values of the computed r from the experimental data at 350 and 300 mA, respectively, as in Table III in the Appendix, together with the rest of the physical constants, we find $\Delta G_{expt} = 124.3\ \text{kJ mol}^{-1}$. This value is very close to our DFT calculation value of $123.24\ \text{kJ mol}^{-1}$. This implies that the reaction paths that are shown in our DFT calculations indeed corresponds to the actual degradation of silicone under high temperature and humidity conditions, and the quantitative model in Eq. (1) indeed shows the degradation process accordingly.

With this model, we can determine the drive current for the LEDs under study so that its lifetime can be longer under the high temperature and humidity condition. We performed another experiment using the same LEDs and the drive current is reduced to 250 mA. Again, we found that Eq. (1) is a good fit to the data, and also the value of A_1indeed varies linearly with the light intensity, which is directly proportional to the drive current as shown in Fig. 3(a).

If we rewrite Eq. (1), we should also expect a straight line that passes through the origin if we plot $\ln\left(\frac{A_d}{A_2}+1\right)$ vs time. Figure 3(b) indeed shows such a straight line for all the three different drive currents. The slope of the line will be the value of A_1. One can see that when the drive current is reduced to 250 mA, its degradation rate reduces significantly.

Since, A_1 can be obtained easily from Fig. 3(a), one can also determine the time when a specific discolored area is reached for different drive current, provided the quality of the silicone can be known. This quality index A_2 can be found experimentally by recording the small observed area of discoloration and the time of occurrence at an early operation time. As, $y = \ln\left(\frac{A_d}{A_2}+1\right) = A_1 t$ in Fig. 3(b), one can determine the y with the time of occurrence determined, and with the measured small area of discoloration, the quality index A_2 can be determined. As the entire model represented by Eq. (1) can now be obtained, the time to reach a certain discolored area in the future can be determined easily and ascertain the reliability of individual LED.

IV. CONCLUSIONS

The degradation mechanisms of PDMS by hydrolysis and condensation in high-power LED housing applications is a major cause of lumen degradation, and the mechanisms were investigated in this work using *ab initio* density function theory methods. The activation energy for the reaction is found to be $123.24\ \text{kJ mol}^{-1}$, which agrees well with the experimental results. The main stressors for the degradation are found to be the humidity and the light that come from the LED chip itself.

From the detailed understanding of the physics of the degradation mechanisms of PDMS under the combined light and humidity, a mathematical model is developed, and the model fits very well to the experimental data at different light intensities. Our model also predicts no degradation if no light is present, which was observed by previous experimental work. This model allows us to predict LED housing discoloration in the future, and it also allows us to quantify the quality of the PDMS housing, which is a factor that will affect the variation of the degradation time of LEDs.

AUTHORS' CONTRIBUTIONS

C.M.T. and A.S. contributed equally to this work.

ACKNOWLEDGMENTS

The authors would like to thank P. Singh for insightful discussions and L. J. Hung for assistance in measurements. They also acknowledge support from the Ministry of Science and Technology, Taiwan (No. MOST 108-2221-E-182-027).

The authors declare no competing financial interests.

APPENDIX: DETAIL DESCRIPTIONS OF METHODS USED AND DERIVATION OF MATHEMATICAL MODEL

1. Methods

a. Ab initio methods

Modeling of PDMS structures in this work is done using a ball and stick model in the MedeA molecular Builder in VASP with its optimization and calculation of thermodynamic properties using the molecular orbital package (MOPAC) where the PM7 method is used for the calculation of Hamiltonian[51–53] for hydrolysis and condensation reactions. The initial and final structures (i.e., reactants and products) of hydrolysis and condensation reactions are designed with the insight from the reported work of Ducom *et al.*[54] where three types of linear PDMS, a methyl terminated, a hydroxyl

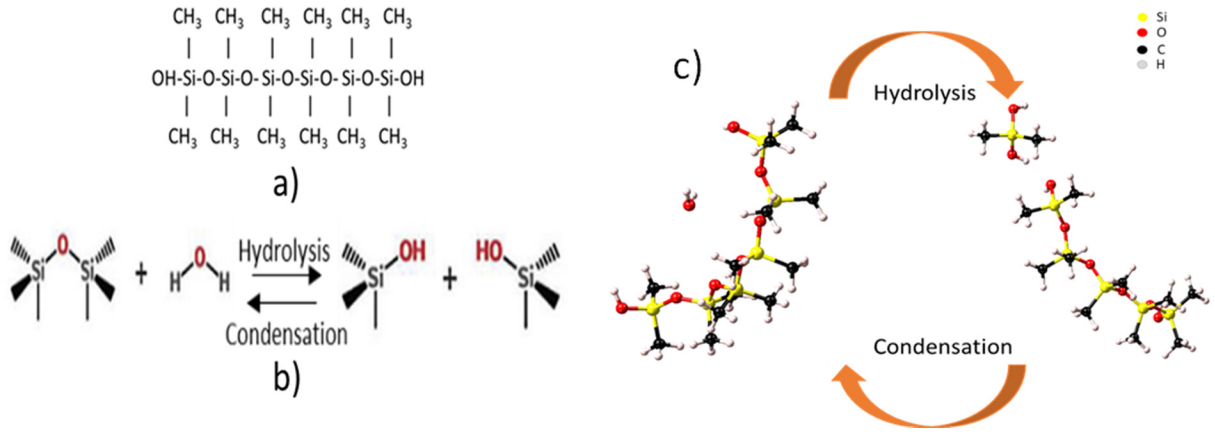

FIG. 4. (a) Structure of the PDMS used in most LED encapsulations and housings.[29–32] (b) Hydrolysis and condensation reactions of the PDMS under the humid condition.[22] Reproduced with permission from Singh and Tan, Opt. Mater. **86**, 148–154 (2018). Copyright 2018 Elsevier B.V. (c) PDMS structures used in this work represented with the ball and stick model.

terminated, and a vinyl terminated polymer, were reported. The structure of hydroxyl terminated polydimethylsiloxane polymer containing six Si atoms, which is also known as dodecamethyl-1,11-pentasiloxanediol, is used in this investigation for the sake of simplicity. The generalized gradient approximation with the Perdew–Burke–Ernzerhof (GGA-PBE) exchange–correlation functional is implemented for describing the interactions,[55] and the structures are equilibrated with DFT theory using the first-principles method.

For the PDMS structure model shown in Fig. 4, the plane wave cutoff energy is taken to be 400 eV, which is found to be a good trade-off between the required computation resources and accuracy. The electronic iterations convergence is 1.00×10^{-5} eV using the normal (blocked Davidson) algorithm and real space projection operators. A $1 \times 1 \times 1$ k-point mesh for Brillouin zone sampling is used where the k-spacing is 0.5 per Angstrom, which corresponds to an actual k-point spacing of $0.419 \times 0.419 \times 0.251$ per Angstrom. The k-mesh is forced to be centered on the gamma point and Gaussian smearing is used which is ideal for semiconductors and insulators. The nudged elastic band (NEB) method is used in MedeA transition state search (TSS) module to map the minimum energy path (MEP) between the initial and the final systems by calculating energy barriers at different points as the energy differences per mole per cell between the starting structure and reaction intermediates.[56,57] The image closest to a saddle point is allowed to climb up into the saddle point (CNEB method) if the largest force on an atom is smaller than 1.0 eV $Å^{-1}$. The self-consistent field (SCF) is calculated by the RMM_DIIS minimizer method.[58] The SCF of each iteration starts from the wave functions of the previous iteration. Diagonal elements of the inverse Hessian are initially set to 0.001 $Å^2$ eV^{-1}. The intermediates of the reactions are created from linear interpolation. The reaction coordinate is the normalized coefficient of linear interpolation with translation criterion of 0.5. Transition states (TSs) are searched with five image points between the initial and final configurations. It is flexible for the user to choose any number of image points for the TS simulation (TSS).

b. Experimental methods

To verify the above model in Eq. (1), four white OSRAM Golden Dragon LEDs are chosen for experimentation. All the LEDs are pre-conditioned in an oven at 125 °C for 3 h before initial measurements to remove possible moisture present in the package initially, which can cause random errors in the experimental results. Initial measurements, including visual material inspection, electrical measurements, spectral power distribution (SPD) measurement, and temperature profiling, are performed. Visual material inspection is done using a Keyence VHX5000 microscope; electrical measurements were done using a Tektronix 2461 Sourcemeter; a TeraLED integrating sphere is used for spectral power distribution of LEDs; and temperature profiling is carried out using a CHCT P384A3-20 thermal scanning system.

The LEDs are divided into two groups with two LEDs in each group, and different drive currents are provided to the LEDs for each group. All the LEDs are subjected to 85 °C/85% RH test condition in a temperature–humidity controlled chamber KD-162-FUL from KING DESIGN. Two different constant currents of 350 and 300 mA are chosen. Optical examination and SPD measurement of the LEDs are performed every 24 h, and the tests are terminated before the crack line is observed for each set because our focus here is to investigate the initial stage of degradation due to hydrolysis and condensation of PDMS. The formation of a crack line indicates the degradation beyond condensation as verified by the work of Singh *et al.*[22]

2. Derivation of the mathematical model of the growth of the area of discoloration with time

Consider an incremental time Δt, and the corresponding increase in V_d is ΔV_d. The ambient temperature will provide thermal energy of K_BT for the entire package, and for an

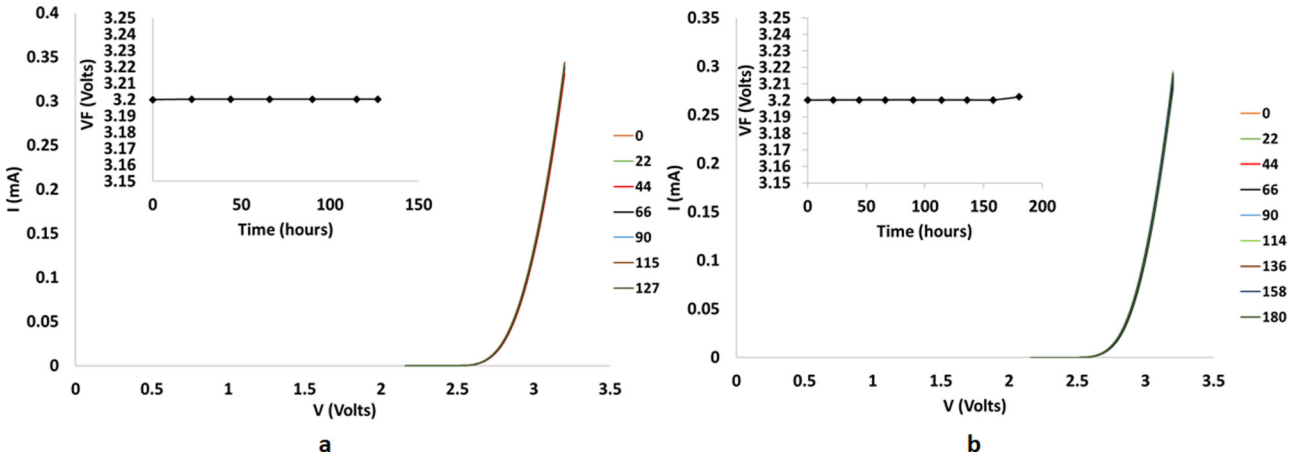

FIG. 5. IV curves of LEDs at (a) 350 mA drive current and (b) 300 mA drive current over test time. The inset of the images shows the variation of VF over time.

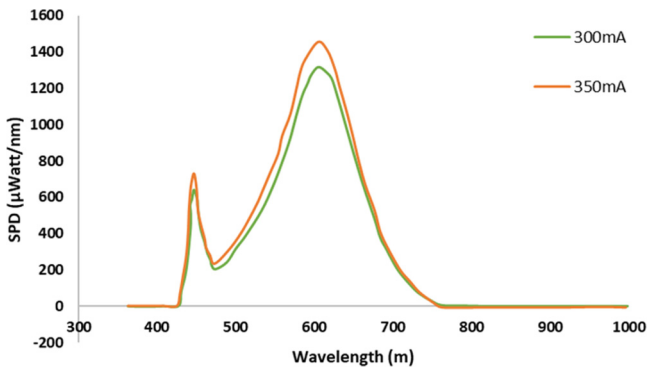

FIG. 6. Spectral power distribution (SPD) curves of LEDs subjected to different input currents before the start of the test.

incremental ΔV_d, the supplied thermal energy will be $K_B T(\Delta V_d/V)$, where V is the total silicone package volume.

The amount of absorption by the discolored volume will be different for different wavelength and can be written as Eq. (A1),

$$E_{light} = \left(\sum_{i=1}^{2} \beta_i P_i\right) V_d \Delta t. \tag{A1}$$

Here, P_1 represents the power density of the blue light and P_2 represents the power density of the yellow light. The corresponding β represents the absorption coefficient of the different light by the discolored region, which we assumed to be constant in this work. As the discolored region is dark brown in color, we can consider all the blue light is absorbed, i.e., $\beta_1 = 1$. The very initial absorption of the lights could be due to the defects in silicone or trapped water molecules in the silicone.[59]

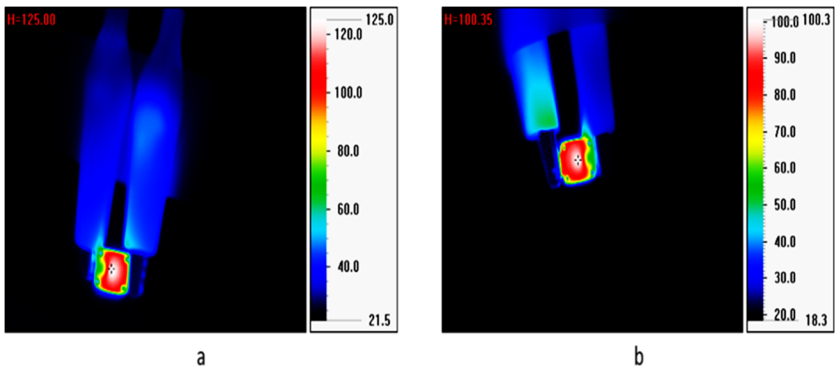

FIG. 7. Temperature distribution of fresh LEDs tested at (a) 350 mA and (b) 300 mA measured using an IR camera (CHCT P384A3-20 thermal scanning system).

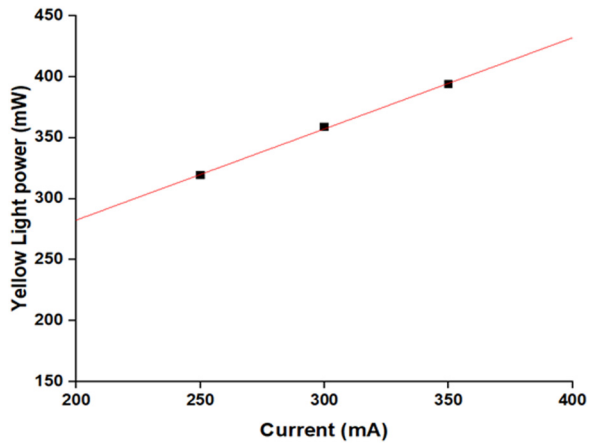

FIG. 8. Plot of P_2 vs drive current.

α_{cond} is denoted as the heat released from condensation reaction per unit volume of the hydrolyzed PDMS and β_3 represents the fraction of α_{cond} that will contribute to the subsequent hydrolysis. When the rate of hydrolysis is slow initially, some of the heat released from condensation will be dissipated to the ambient, and $\beta_3 < 1$. At a later time, where the rate of hydrolysis becomes fast, $\beta_3 \to 1$ since the rate of heat dissipation to the ambient will be slower than the rate of absorption by the hydrolysis reaction. In other words, β_3 is not a constant with time. ΔV_d is denoted as the incremental volume of the discolored region in the immediate past hydrolysis reaction, where the subsequent condensation reaction occurs, and the energy supplied from the condensation reaction is given by Eq. (A2),

$$E_{cond} = \alpha_{cond}\beta_3\Delta V_d. \tag{A2}$$

Therefore, within Δt, the total energy given for the hydrolysis reaction is given in Eq. (A3),

$$E_{total} = \sum_{i=1}^{2}\beta_i P_i V_d \Delta t + k_B T\frac{\Delta V_d}{V} + \alpha_{cond}\beta_3\Delta V_d. \tag{A3}$$

As the activation energy for the hydrolysis is $E_a = 123.3$ kJ/mol, the amount of new discolored volume due to this total energy will be proportional to E_{total}/E_a, which can be expressed in Eq. (A4), where k_1 is the proportional constant,

$$\frac{\left(\sum_{i=1}^{2}\beta_i P_i V_d\Delta t + k_B T\frac{\Delta V_d}{V} + \alpha_{cond}\beta_3\Delta V_d\right)}{E_a} = k_1\Delta V_d. \tag{A4}$$

Equation (A4) can be rewritten as Eq. (A5), and its solution is given in Eq. (A8),

$$\frac{dV_d}{dt} = A_1 V_d, \tag{A5}$$

$$A_1 = \frac{\sum_{i=1}^{2}\beta_i P_i}{\alpha}, \tag{A6}$$

$$\alpha = k_1 E_a - \frac{k_B T}{V} - \alpha_{cond}\beta_3, \tag{A7}$$

$$V_d(t) = V_0 e^{A_1(t-t_0)} = A_2 e^{A_1 t}. \tag{A8}$$

At time zero, V_d should be close to zero, and Eq. (A8) should be modified accordingly as in Eq. (A9) with $A_0 \approx -A_2$,

$$\mathrm{V_d(t)} = \mathrm{A_0} + \mathrm{A_2 e^{A_1 t}}. \tag{A9}$$

From Eq. (A8), we can see that $A_2 = V_0 e^{-A_1 t_0}$, and t_0 is the incubation time for the formation of discoloration, i.e., it is the time needed to accumulate sufficient hydrolysis by-product to begin the discoloration and the corresponding discolored volume is V_0. If the silicone has larger defects that can absorb light for the initiation of hydrolysis, then the incubation time will be smaller. In other words, A_2 represents the quality of the silicone. The poorer the quality, the larger its value.

For experimental verification, to observe the continuous growth of the discolored regions, we can only observe them optically without any cross section, and thus its volume cannot be determined. By assuming a constant thickness of the region, which

TABLE II. Values of the model Parameters for the best fit of the average A_d from the LEDs.

Current (mA)	A_0	A_1	A_2	Regression coefficient
350	−0.457	0.0217	0.457	1
300	−0.910	0.0105	0.966	0.986

TABLE I. Temperatures of LEDs at different input currents and related energies.

Current (mA)	Total LED temperature measured at 25 °C, $T_{measured}$ (°C)	LED chip temperature due to drive current, $T_{led} = T_{measured} - T_{room}$ (°C)	Ambient test temperature, $T_{chamber}$ (°C)	Total LED temperature, T_{total} (K)	Energy from temperature, E_K (kJ mol^{-1})
350	125	100	85	458	5.71
300	100.3	75.3	85	433.3	5.4

TABLE III. Calculation of rate of reaction (r) and activation energy (ΔG_{expt}) from experimental results.

Current (mA)	Total LED temperature (T_{total}) (K)	Time to discoloration (t) (h)	Discolored area (A_d) (mm^2)	Rate of reaction (r) (mm^2 h^{-1})	Activation energy as computed from Eq. (2) (ΔG_{expt}) (kJ mol^{-1})
350	458	127	8.04	0.063	124.3
300	433.3	180	6.02	0.033	120

is approximately equal to the reciprocal of the effective attenuation coefficients of the blue and yellow lights from the LEDs, we can modify Eq. (A9) as Eq. (A10),

$$A_d(t) = A'_0 + A'_2 e^{A'_1 t}. \quad \text{(A10)}$$

The values of A'_0, A'_1, and A'_2 will be their corresponding values in Eq. (A9) divided by the effective penetration depth of the light.

3. Model development

Electrical measurement analysis was performed for all the LEDs under test over the period of test time as shown in Fig. 5. It is evident that maximum forward voltage (V_F) remains constant over the test time, which indicates that die attached delamination, change in the thermal resistance, or chip degradation has not occurred in our LEDs during the specified test time.[60] Hence, the effect of junction temperature in the degradation of LEDs under test during early degradation time can be omitted.

SPD measurements result for each set of LEDs at different input currents are as shown in Fig. 6. The y axis is the spectral power distribution (SPD), which is the power per unit wavelength of an illumination. We can see that the power per unit wavelength of the LEDs decreases with the drive current as expected.

Due to the less than perfect phosphor conversion, when the blue light is converted into yellow light, some heat energy will be resulted. Figure 7 and Table I show our measurement of the LED temperatures when the blue light intensity changes due to the change in the drive current (Table IV).

4. Model verification

Example of rate of reaction calculation: for 350 mA supplied drive current, the area of discoloration was found to be 8.04 mm^2 after 127 h. Thus, the rate of reaction r = area of discoloration/time to discoloration = 0.063 mm^2 h^{-1}.

TABLE IV. Calculation of blue and yellow light power at different drive currents by deconvolution and calculation of areas under curve from Fig. 6.

Current (mA)	Blue (mW)	Yellow (mW)	Total (mW)
350	23.0	393.8	416.8
300	33.8	358.8	392.6
250	33.7	319.1	352.8

We find that the yellow light power (P_2) increases with light intensity, which is linearly dependent on the drive current of the LEDs. The linear behavior of Fig. 8 indeed indicates that the constant A_1 in Eq. (A10) also increases linearly with drive current as A_1 as observed experimentally and shown in is Fig. 3(a) of the main text. A_1 is a cumulative function of light intensities given by Eq. (A6), but $P_2 \gg P_1$ as shown in Table IV; thus, only the variation of P_2 with the drive current is reflected in the variation of A_1 with the current. This observation makes it evident that the rapid increase of discoloration in the silicone housing is driven by the intensity of phosphor converted yellow light in LEDs.

DATA AVAILABILITY

The data that support the findings of this study are available from the corresponding author upon reasonable request.

REFERENCES

[1]See https://www.energy.gov/eere/ssl/articles/us-department-energy-publishes-new-energy-savings-forecast-solid-state-lighting for "U.S. Department of Energy publishes new energy savings forecast for solid-state lighting."
[2]T. Abergel, "International Energy Agency;" available at https://www.iea.org/reports/lighting.
[3]See https://www.1ledlight.com/chinas-led-lighting-fixtures-are-frequently-recalled-and-quality-problems-constrain-international-competitiveness.html for "China's LED lighting fixtures are frequently recalled, and quality problems constrain international competitiveness."
[4]See https://www.cpsc.gov/Recalls/2014/halco-recalls-led-bulbs for "Halco recalls LED bulbs due to risk of injury and burn hazards."
[5]See https://www.cpsc.gov/Recalls/2018/cooper-lighting-recalls-solarbattery-powered-light-fixtures-due-to-fire-hazard for "Cooper lighting recalls solar/battery powered light fixtures due to fire hazard."
[6]C. Ferretti, "Detroit's LED streetlights going dark after a few years" (2019); available at https://www.detroitnews.com/story/news/local/detroit-city/2019/05/07/detroits-led-streetlights-going-dark-after-few-years/3650465002/.
[7]C. H. Wang, S. P. Chang, P. H. Ku, J. C. Li, Y. P. Lan, C. C. Lin, H. C. Yang, H. C. Kuo, T. C. Lu, S. C. Wang, and C. Y. Chang, "Hole transport improvement in InGaN/GaN light-emitting diodes by graded-composition multiple quantum barriers," Appl. Phys. Lett. **99**, 2009–2012 (2011).
[8]C. H. Wang, S. P. Chang, W. T. Chang, J. C. Li, Y. S. Lu, Z. Y. Li, H. C. Yang, H. C. Kuo, T. C. Lu, and S. C. Wang, "Efficiency droop alleviation in InGaN/GaN light-emitting diodes by graded-thickness multiple quantum wells," Appl. Phys. Lett. **97**, 95–98 (2010).
[9]Y. K. Kuo, J. Y. Chang, M. C. Tsai, and S. H. Yen, "Advantages of blue InGaN multiple-quantum well light-emitting diodes with InGaN barriers," Appl. Phys. Lett. **95**, 011116 (2009).
[10]P. T. Barletta, E. A. Berkman, B. F. Moody, N. A. El-Masry, A. M. Emara, M. J. Reed, and S. M. Bedair, "Development of green, yellow, and amber light emitting diodes using InGaN multiple quantum well structures," Appl. Phys. Lett. **90**, 151109 (2007).

[11]H. Daicho, T. Iwasaki, K. Enomoto, Y. Sasaki, Y. Maeno, Y. Shinomiya, S. Aoyagi, E. Nishibori, M. Sakata, H. Sawa, S. Matsuishi, and H. Hosono, "A novel phosphor for glareless white light-emitting diodes," Nat. Commun. **3**, 1132 (2012).
[12]L. Chen, C.-C. Lin, C.-W. Yeh, and R.-S. Liu, "Light converting inorganic phosphors for white light-emitting diodes," Materials **3**, 2172–2195 (2010).
[13]J. Cho, J. H. Park, J. K. Kim, and E. F. Schubert, "White light-emitting diodes: History, progress, and future," Laser Photonics Rev. **11**, 1600147 (2017).
[14]J. K. Kim, H. Luo, E. F. Schubert, J. Cho, C. Sone, and Y. Park, "Strongly enhanced phosphor efficiency in GaInN white light-emitting diodes using remote phosphor configuration and diffuse reflector cup," Jpn. J. Appl. Phys. **44**, 19–22 (2005).
[15]C. C. Lin and R.-S. Liu, "Advances in phosphors for light-emitting diodes," J. Phys. Chem. Lett. **2**, 1268–1277 (2011).
[16]L. E. D. Chip, P. With, B. Green, G. C. Chi, and R. K. Wu, "White-light emission from near UV InGaN–GaN," Technology **15**, 18–20 (2003).
[17]S. Ye, F. Xiao, Y. X. Pan, Y. Y. Ma, and Q. Y. Zhang, "Phosphors in phosphor-converted white light-emitting diodes: Recent advances in materials, techniques and properties," Mater. Sci. Eng.: R: Rep. **71**, 1–34 (2010).
[18]H. Luo, J. K. Kim, E. F. Schubert, J. Cho, C. Sone, and Y. Park, "Analysis of high-power packages for phosphor-based white-light-emitting diodes," Appl. Phys. Lett. **86**, 1–3 (2005).
[19]N. A. Diachun, A. H. Marcus, D. M. Hussey, and M. D. Fayer, "Dynamics in polydimethylsiloxane: The effect of solute polarity," J. Am. Chem. Soc. **116**, 1027–1032 (1994).
[20]C. Rücker and K. Kümmerer, "Environmental chemistry of organosiloxanes," Chem. Rev. **115**, 466–524 (2015).
[21]F. M. Lewis, "The science and technology of silicone rubber," Rubber Chemistry and Technology 35(5), 1222–1275 (1962).
[22]P. Singh and C. M. Tan, "Time evolution of packaged LED lamp degradation in outdoor applications," Opt. Mater. **86**, 148–154 (2018).
[23]P. Singh and C. M. Tan, "Degradation physics of high power LEDs in outdoor environment and the role of phosphor in the degradation process," Sci. Rep. **6**, 1–13 (2016).
[24]P. Singh and C. M. Tan, "A review on the humidity reliability of high power white light LEDs," Microelectron. Reliab. **61**, 129–139 (2016).
[25]R. G. Parr, N. Handy, N. March, P. Payne, L. Samuels, and W. Wang, in *Density-Functional Theory of Atoms and Molecules* (Springer, 1989), pp. 5–15.
[26]A. Aliano and G. Cicero, *Encyclopedia of Nanotechnology* (Springer Science +Business Media, B.V. 2012).
[27]J. Hafner, C. Wolverton, and G. Ceder, "Toward computational materials design: The impact of density functional theory on materials research," MRS Bull. **31**, 659–668 (2006).
[28]G. Kresse and J. Hafner, "*Ab initio* molecular dynamics for liquid metals," Phys. Rev. B **47**, 558–561 (1993).
[29]L. Nian, X. Pei, Z. Zhao, and X. Wang, "Review of optical designs for light-emitting diode packaging," IEEE Trans. Compon. Packag. Manuf. Technol. **9**, 642–648 (2019).
[30]Y.-K. Su, P. C. Wang, C. L. Lin, G. S. Huang, and C. M. Wei, "Enhanced light extraction using blue LED package consisting of TiO_2-doped silicone layer and silicone lens," IEEE Electron Device Lett. **35**, 575–577 (2014).
[31]D. D. Li, S. Li, S. Zhang, X. W. Liu, and C. P. Wong, "Thermo and dynamic mechanical properties of the high refractive index silicone resin for light emitting diode packaging," IEEE Trans. Compon. Packag. Manuf. Technol. **4**, 190–197 (2014).
[32]A. W. Norris, M. Bahadur, and M. Yoshitake, "Novel silicone materials for LED packaging," Proc. SPIE **5941**, 594115 (2005).
[33]W. Klopper, J. G. C. M. Van Duijneveldt-van De Rijdt, and F. B. Van Duijneveldt, "Computational determination of equilibrium geometry and dissociation energy of the water dimer," Phys. Chem. Chem. Phys. **2**, 2227–2234 (2000).
[34]M. Cypryk and Y. Apeloig, "Mechanism of the acid-catalyzed Si-O bond cleavage in siloxanes and siloxanols. A theoretical study," Organometallics **21**, 2165–2175 (2002).
[35]C. Technology, "Glass ceramics," J. Am. Ceramic Society-Wiederhorn and Bolz **53**(10), 2–3 (1970).
[36]N. W. Taylor, "Mechanism of fracture of glass and similar brittle solids," J. Appl. Phys. **18**, 943–955 (1947).
[37]D. A. Stuart and O. L. Anderson, "Dependence of ultimate strength of glass under constant load on temperature, ambient atmosphere, and time," J. Am. Ceram. Soc. **36**, 416–424 (1953).
[38]W. W. Gerberich and M. Stout, "Discussion of thermally activated approaches to glass fracture," J. Am. Ceram. Soc. **59**, 222–225 (1976).
[39]B. K. Atkinson, "A fracture mechanics study of subcritical tensile cracking of quartz in wet environments," Pure Appl. Geophys. **117**, 1011–1024 (1979).
[40]C. Hühn, A. Erlebach, D. Mey, L. Wondraczek, and M. Sierka, "*Ab initio* energetics of Si—O bond cleavage," J. Comput. Chem. **38**, 2349–2353 (2017).
[41]P. Ptáček, F. Šoukal, and T. Opravil, "Introduction to the Transition state theory," in *Introducing the Effective Mass of Activated Complex and the Discussion on the Wave Function of this Instanton* (Intech, 2018).
[42]J. K. West, "Theoretical analysis of hydrolysis of polydimethylsiloxane (PDMS)," J. Biomed. Mater. Res. **35**, 505–511 (1997).
[43]C. A. Ballhausen and H. B. Gray, *Molecular Orbital Theory: An Introductory Lecture Note and Reprint Volume* (W. A. Benjamin, Inc., 2006).
[44]J. Spivack and S. B. Dorn, "Hydrolysis of oligodimethylsiloxane-α,ω-diols and the position of hydrolytic equilibrium," Environ. Sci. Technol. **28**, 2345–2352 (1994).
[45]Y. Demirel, "Extended nonequilibrium thermodynamics," in *Nonequilibrium Thermodynamics* (Elsevier, 2002), Vol. V, pp. 373–394.
[46]S. Varaprath, D. H. Stutts, and G. E. Kozerski, "A primer on the analytical aspects of silicones at trace levels-challenges and artifacts—A review," Silicon Chem. **3**, 79–102 (2006).
[47]C. Kapridaki and P. Maravelaki-Kalaitzaki, "TiO_2-SiO_2-PDMS nanocomposite hydrophobic coating with self-cleaning properties for marble protection," Prog. Org. Coat. **76**, 400–410 (2013).
[48]K. Hood, *Comprehensive Polymer Science and Supplements* (Elsevier, 1989).
[49]F. G. Helfferich, "Chapter 12—Unusual thermal and mass-transfer effects," Compr. Chem. Kinet. **38**, 375–388 (2001).
[50]M. G. Evans and M. Polanyi, "Some applications of the transition state method to the calculation of reaction velocities, especially in solution" Transactions of the Faraday Society **31**, 875–894 (1935).
[51]H. Jürgen, "Materials simulations using VASP—a quantum perspective to materials science," Computer physics communications **177**(1–2), 6–13 (2011).
[52]G. Kresse and J. Furthmüller, "Efficient iterative schemes for *ab initio* total-energy calculations using a plane-wave basis set," Phys. Rev. B **54**, 11169–11186 (1996).
[53]J. J. P. Stewart, "Optimization of parameters for semiempirical methods VI: More modifications to the NDDO approximations and re-optimization of parameters," J. Molecular Modeling **19**(1), 1–32 (2013).
[54]G. Ducom, B. Laubie, A. Ohannessian, C. Chottier, P. Germain, and V. Chatain, "Hydrolysis of polydimethylsiloxane fluids in controlled aqueous solutions," Water Sci. Tech. **68**(4), 813–820 (2013).
[55]G. K. H. Madsen, "Functional form of the generalized gradient approximation for exchange: The PBEα functional," Phys. Rev. B **75**, 195108 (2007).
[56]G. Henkelman, B. P. Uberuaga, and H. Jónsson, "Climbing image nudged elastic band method for finding saddle points and minimum energy paths," J. Chem. Phys. **113**, 9901–9904 (2000).
[57]G. Henkelman, G. Jóhannesson, and H. Jónsson, "Methods for finding saddle points and minimum energy paths," in *Theoretical Methods in Condensed Phase Chemistry* (Kluwer Academic Publishers, 2005), pp. 269–302.
[58]T. Rohwedder and R. Schneider, "An analysis for the DIIS acceleration method used in quantum chemistry calculations," J. Math. Chem. **49**, 1889–1914 (2011).
[59]C. M. Tan, B. K. Chen, X. Li, and S. J. Chen, "Rapid light output degradation of GaN-based packaged LED in the early stage of humidity test," IEEE Trans. Device Mater. Reliab. **12**, 44–48 (2012).
[60]C. M. Tan and P. Singh, "Time evolution degradation physics in high power white LEDs under high temperature-humidity conditions," IEEE Trans. Device Mater. Reliab. **14**, 742–750 (2014).